analytical chemistry

Article

pubs.acs.org/ac

Real-Time Viscosity and Mass Density Sensors Requiring Microliter Sample Volume Based on Nanomechanical Resonators

Benjamin A. Bircher,[†] Luc Duempelmann,[†] Kasper Renggli,[‡] Hans Peter Lang,[§] Christoph Gerber,[§] Nico Bruns,[‡] and Thomas Braun*[,†]

[†]Center for Cellular Imaging and NanoAnalytics, Biozentrum, University of Basel, Mattenstrasse 26, CH-4058 Basel, Switzerland

[‡]Department of Chemistry, University of Basel, Klingelbergstrasse 80, CH-4056 Basel, Switzerland

[§]Swiss Nanoscience Institute, University of Basel, Klingelbergstrasse 82, CH-4056 Basel, Switzerland

Supporting Information

ABSTRACT: A microcantilever based method for fluid viscosity and mass density measurements with high temporal resolution and microliter sample consumption is presented. Nanomechanical cantilever vibration is driven by photothermal excitation and detected by an optical beam deflection system using two laser beams of different wavelengths. The theoretical framework relating cantilever response to the viscosity and mass density of the surrounding fluid was extended to consider higher flexural modes vibrating at high Reynolds numbers. The performance of the developed sensor and extended theory was validated over a viscosity range of 1−20 mPa·s and a corresponding mass density range of 998−1176 kg/m^3 using reference fluids. Separating sample plugs from the carrier fluid by a two-phase configuration in combination with a microfluidic flow cell, allowed samples of 5 μL to be sequentially measured under continuous flow, opening the method to fast and reliable screening applications. To demonstrate the study of dynamic processes, the viscosity and mass density changes occurring during the free radical polymerization of acrylamide were monitored and compared to published data. Shear-thinning was observed in the viscosity data at higher flexural modes, which vibrate at elevated frequencies. Rheokinetic models allowed the monomer-to-polymer conversion to be tracked in spite of the shear-thinning behavior, and could be applied to study the kinetics of unknown processes.

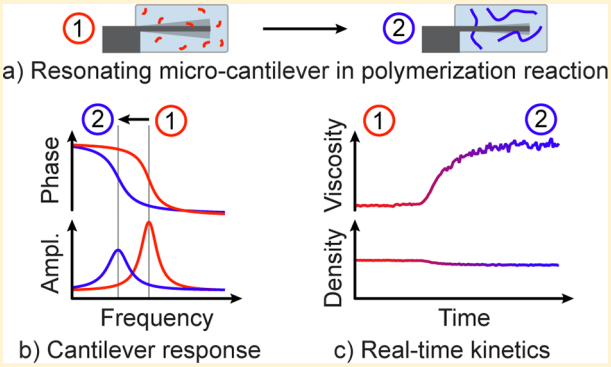

Viscosity and mass density are key characteristics of fluids. They depend on the solvent, as well as on the physicochemical properties of the dissolved components. Viscosity measurements are used to characterize solutions of polymers and biopolymers.[1] Whereas the density is mainly related to concentration and hydrodynamic volume, the viscosity depends on concentration, molecular weight, shape, and interactions of the solute molecules. Classical viscosity or mass density measurements require milliliter samples with a time resolution of the order of minutes. Recently, new sensing methods that allow either microfluidic viscosity[2] or mass density[3,4] measurements were presented. Notably, most of these new viscosity measurement techniques rely on fluorescent labels or optical readout and subsequent image processing. In contrast, combined viscosity and mass density sensing methods are mostly based on mechanical resonators. They employ resonating microtubes,[5] microelectromechanical systems,[6] surface acoustic wave devices,[7] tuning forks,[8] quartz crystal microbalances,[9] and microcantilevers.[10] Because of the wide application range of microcantilevers in scanning probe microscopy, comprehensive theoretical frameworks considering arbitrary modes of vibration have been developed[11,12] and experimentally tested.[10,13−15] Reported applications include characterization of polymer solutions,[16] concentration determination of sugar solutions,[17] and viscosity measurements of hydrocarbons and silicone oils[18] and ethanol solutions.[19,20] A comprehensive review on fluidic applications using microcantilevers is given by Kim et al.[21] Only few papers report time-resolved changes in cantilever resonance parameters in fluids, resulting from viscosity and mass density variations.[22,23] Furthermore, reviewing viscosity and mass density data measured using microcantilevers led us to the conclusion that careful calibration and a vibrational spectrum without spurious resonance peaks are essential to achieve good accuracy.

In this paper, we use resonating nanomechanical cantilevers embedded in a microliter fluid cell as transducers for real-time viscosity and mass density measurements. Photothermal excitation of the cantilever was implemented, and the use of higher flexural modes of vibration was studied. The performance of the instrument was evaluated using glycerol solutions. A segmented two-phase flow allowed sequential measurements to

Received: May 17, 2013
Accepted: August 1, 2013
Published: August 1, 2013

   dx.doi.org/10.1021/ac4014918 | *Anal. Chem.* 2013, 85, 8676−8683

be performed using sample volumes as low as 5 μL. Subsequently, the use of the method to monitor polymerization reaction kinetics with microliter sample consumption was investigated.

MATERIALS AND METHODS

Unless otherwise indicated, nanopure water was used and chemicals were purchased from Sigma-Aldrich (Buchs, Switzerland) and used without further purification.

Experimental Setup. The experimental setup employed to excite and detect higher flexural mode cantilever vibrations in liquid is shown in Figures 1a and b. By sweeping given ranges of frequencies (sweep time 1.0 to 1.67 s), amplitude and phase spectra of arbitrary flexural modes are recorded on a vector network analyzer (MS4630B, Anritsu, Kanagawa, Japan). The reference signal is applied to the excitation laser driving the cantilever (LD_{EX}, 406 nm, 4.4 mW_{DC}, peak-to-peak modulation amplitude 7.0 mW_{pp} at the output aperture of the objective; LP406-SF20, Thorlabs, Newton, New Jersey, U.S.A.). The dynamic response is monitored using the detection laser (LD_{DE}, 780 nm, 0.8 mW_{DC}; 51nanoFCM-H06, Schäfter + Kirchhoff GmbH, Hamburg, Germany), which is reflected off the free end of the cantilever. The optical deflection signal is directed onto a position-sensitive detector (PSD, 2L10_SU7, SiTek Electro Optics, Partille, Sweden); a motorized translational stage keeps the laser spot centered on the PSD. Photocurrents from two opposing electrodes on the PSD are converted by home-built transimpedance amplifiers (bandwidth = 850 kHz) and fed into a differential amplifier (gain = 10×; SIM910/SIM911, Stanford Research Systems, Sunnyvale, CA, U.S.A.; or DA1822, Teledyne LeCroy, Chestnut Ridge, NY, U.S.A.). The differential signal is fed back into the network analyzer (lock-in bandwidth = 300/500 Hz) and divided by the signal originating from a reference photodiode (PD, PDA36A, Thorlabs, Newton, New Jersey, U.S.A.). Specifically developed, object-oriented LabVIEW software (National Instruments, Austin, Texas, U.S.A.) is used to control and record data from the network analyzer. Amplitude and phase spectra are recorded and saved consecutively. A Lorentzian curve fitting routine allows resonance frequencies and quality factors to be tracked in real-time. Furthermore, the software monitors the deflection and intensity of the signal on the position-sensitive detector, stabilizes the temperature of the fluid cell to 20 ± 0.01 °C, and controls the valve and syringe pump used for sample injection.

Fluid Cell and Sample Injection. A syringe pump (KDS900, KD Scientific, Holliston, MA, U.S.A.) and a ten port valve (VV-C2H-1340EH, VICI, Schenkon, Switzerland) equipped with two sample loops (10 and 50 μL) allow sequential injection of samples into the fluid cell using a carrier fluid, either water or hydrocarbon oil, at flow rates between 0.1 and 50 μL/min (Figure 1c). To monitor a polymerization process in an external vessel, sample is aspirated into the fluid cell as illustrated by Figure 1d. All measurements are performed under continuous flow. The parts are connected with polyether ether ketone (PEEK) tubes (inner diameter 250 μm). The fluid cell (volume <2 μL) is molded in polydimethylsiloxane (PDMS).[24] The required master template was produced from a cantilever chip body and a glass rod (diameter 1 mm) glued to a microscopy glass slide. Replica are fabricated by pouring degassed PDMS (SYLGARD 184, Dow Corning, Midland, MI, U.S.A.) onto the master template and baking at 60 °C for at least 4 h. After activation in a 30 W oxygen plasma for 30 s

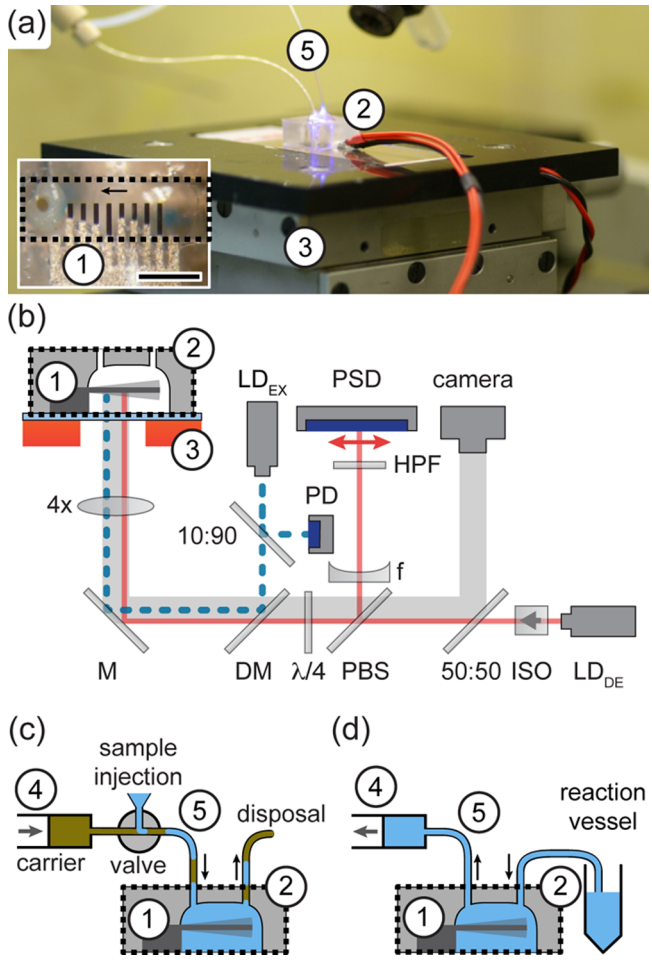

Figure 1. (a) Photograph and (b) schematic diagram of the experimental setup. Inset: Micrograph of the fluid cell; the dotted black line indicates the fluid channel and the arrow the flow direction (scale bar = 1 mm). Configurations of the fluidic setup: (c) Sequential sample injection and (d) sample aspiration from an external vessel. The cantilever chip (1) is integrated in a PDMS fluid cell and (2) mounted on a temperature-controlled stage (3). A syringe pump (4) allows injection or aspiration of sample into the fluid cell through PEEK tubes (5). The beam (dashed blue line, b) from an intensity-modulated excitation laser (LD_{EX}) is split 10:90 between a reference photodiode (PD) and a dichroic mirror (DM), respectively. It is directed upward by a broadband mirror (M) and focused onto the cantilever by an objective lens (4×). To detect the vibration, the reflected beam of the detection laser (LD_{DE}, solid red line, b) originating from the cantilever, is directed through a concave lens (f = −50 mm) onto a position-sensitive detector (PSD), by combining a polarizing beam splitter (PBS) and a lambda-quarter plate ($\lambda/4$). An optical high-pass filter (HPF) is inserted to avoid disturbances on the PSD. An optical isolator (ISO) is used to avoid back reflection into the laser diode. Optical access for a camera is provided by a 50:50 beam splitter.

(PDC-002, Harrick Plasma, Ithaca, NY, U.S.A.), a cantilever chip is inserted and the fluid cell is bonded to a microscopy glass slide. The dimensions of the fluid cell where chosen to ensure that boundary effects, such as squeeze film damping, are negligible.[25]

Cantilever Preparation. Arrays comprised of cantilevers with different lengths (IBM Zurich Research Laboratory, Rueschlikon, Switzerland; nominal dimensions 500/300/250/200 × 100 × 4 μm^3), were cleaned in piranha solution (30%

dx.doi.org/10.1021/ac4014918 | Anal. Chem. 2013, 85, 8676−8683

hydrogen peroxide and 96% sulfuric acid, 1:1) for 30 min, washed four times in water, once in isopropanol and dried in air. To passivate the silicon, cantilevers were incubated in 10 mM 2-(methoxy(polyethyleneoxy)propyl)trimethoxysilane (90%, ABCR, Karlsruhe, Germany) in ethanol for 30 min at room temperature. Subsequently, a 2 nm titanium layer (Johnson Matthey, Zurich, Switzerland) followed by a 20 nm gold layer (Goodfellow, Huntingdon, England) were deposited using an electron-beam evaporator (EVA 300, Alliance Concept, Cran Gevrier, France). The gold layer was then passivated in 1 mM (1-Mercapto-11-undecyl)tetra(ethylene glycol) (95%, ASEMBLON Inc., Redmond, WA, U.S.A.) in ethanol for 30 min at room temperature, washed in water, and rinsed with isopropanol. Cantilevers were stored under argon atmosphere until use. For all experiments, only the cantilevers with the highest aspect ratio were used ($500 \times 100 \times 4\ \mu m^3$).

Glycerol Reference Solutions and Free Radical Polymerization Reaction. Viscosity and mass density standards were prepared from weighed amounts of water and glycerol. The glycerol concentrations ranged from 30.5% to 73.0% (w/w) and corresponding viscosity and mass density values were calculated according to literature.[26,27] The reference solutions were mixed and filtered through a sterile 0.20 μm filter. Water was used as carrier fluid for the reference measurements. A total of 45 μL of each glycerol reference solution was injected into the fluid cell at 5 μL/min (first 15 μL) and measured at 2 μL/min (following 30 μL). Subsequently, the fluid cell was purged with water at 2 μL/min. For segmented two-phase flow experiments a hydrocarbon oil (Viscosity and Density Standard N1.0, 19044; 1.03 mPa·s, 779 kg/m^3) was used as carrier fluid and 5 μL samples were sequentially injected at a constant flow rate of 5 μL/min (see Figure 1c).

To study the free radical polymerization of acrylamide at room temperature in a time-resolved manner, the monomer acrylamide (3.4%, 478 mM, 109 equiv.) and the catalyst tetramethylethylenediamine (TEMED; 6.6 mM, 1.5 equiv.) were dissolved in water and placed in an Eppendorf tube (total sample volume = 1.5 mL). The solution was fed into the fluid cell by aspirating it at a rate of 1 μL/min (see Figure 1d). The polymerization reaction was initiated by adding ammonium persulfate (APS; 4.4 mM, 1 equiv.) and the flow rate was increased to 10 μL/min for 1 min to overcome the dead volume of the connecting tube (~5 μL). Subsequently, the flow rate was decreased to 1 μL/min and kept at this value during the entire reaction (65 min). The total sample consumption during the reaction was 75 μL. As the reaction was carried out in air and the water was not deoxygenated, atmospheric oxygen was present in the reaction mixture and quenched the reaction in the initial phase. The final degree of conversion of the reaction was determined by ^{1}H NMR spectroscopy using a Bruker DPX-NMR (400 MHz) instrument (Bruker, Billerica, MA, U.S.A.). Sample (0.4 mL) was added to 0.4 mL of D_2O (Cambridge Isotope Laboratory Tewksbury, MA, U.S.A.) and analyzed by ^{1}H NMR at room temperature. The degree of conversion was calculated from the baseline corrected spectra using the integrals of the vinyl protons of the monomer and the protons of the polymer backbone.

Data Analysis and Hydrodynamic Forces. The following procedure was followed to measure the viscosity and mass density using a vibrating cantilever immersed in the fluid under test: (i) The eigenfrequency and quality factor of the cantilever were experimentally determined; (ii) the hydrodynamic function, relating these parameters to the viscosity and mass density of the fluid, was solved; (iii) after a calibration step, the fluid properties were determined. To determine the eigenfrequency and quality factor of the cantilever, a damped harmonic oscillator model was fitted to the amplitude and phase spectra individually[28] (see Supporting Information). The hydrodynamic function Γ (see below for details) introduced by Sader and Van Eysden,[11,12] relates the eigenfrequency f_n and quality factor Q_n of a vibrating cantilever to the viscosity and mass density of the surrounding fluid

$$f_n = f_{n,\mathrm{vac}}\left(1 + \frac{\pi w \rho}{4 t \rho_c}\mathcal{R}(\Gamma(Re, \kappa_n))\right)^{-1/2} \quad (1)$$

$$Q_n = C_{n,\mathrm{cal}}\frac{\frac{4t\rho_c}{\pi w \rho} + \mathcal{R}(\Gamma(Re, \kappa_n))}{\mathcal{I}(\Gamma(Re, \kappa_n))} \quad (2)$$

The Reynolds number[12] $Re = 2\pi f_n \rho w^2/\eta$, quantifies inertial against viscous forces and the normalized mode number $\kappa_n = w\alpha_n/L$, is related to the spatial wavelength of the beam. The parameters t, w, L, ρ_c, f_n, and Q_n are the thickness, width, length, average mass density (2330 kg/m^3), eigenfrequency, and quality factor of mode n, with eigenvalue, α_n (see Supporting Information), of the cantilever immersed in a fluid of mass density ρ and viscosity η. The real part $\mathcal{R}(\Gamma)$of the hydrodynamic function describes inertial forces, whereas the imaginary part $\mathcal{I}(\Gamma)$ represents dissipative forces exerted by the fluid. Compressibility of the fluid should be considered when the spatial wavelength of a flexural mode exceeds the acoustic wavelength in the fluid at the corresponding frequency. In aqueous solutions this condition is met for flexural mode numbers above 24 for the cantilevers employed.[29] Because the highest detectable mode is far below this value, compressibility was neglected in the analysis. The employed model furthermore assumes the no-slip boundary condition.[30] Equation 1 is solved by an iterative process,[31] because the hydrodynamic function depends on the eigenfrequency. A calibration step is required to account for uncertainties in the dimensions of the cantilever as well as to compensate for nonideal effects. It is performed in a single reference fluid, water or oil in the present case, at the start of every series of experiments. The calibration factors, the vacuum frequency[10] $f_{n,\mathrm{vac}}$ and the quality factor calibration constant $C_{n,\mathrm{cal}}$, are determined for each flexural mode n by a root-finding algorithm in IGOR Pro (WaveMetrics, Lake Oswego, OR, U.S.A.), using eqs 1 and 2. Once determined, the calibration factors $f_{n,\mathrm{vac}}$ and $C_{n,\mathrm{cal}}$ are used to calculate the viscosity and mass density of the fluid under test.

The approach used to describe the hydrodynamic function Γ is discussed in the following. Higher modes of vibration entail high Reynolds numbers Re due to their elevated eigenfrequencies f_n. The numerical calculation of Γ for such high Re requires a large number of terms to reach convergence,[30] which would demand both very high numerical precision and computing time. Therefore, empirical implementations of Γ have been developed and successfully applied.[33,34] We introduce an approximation, which is valid for $Re \geq 10^3$ and therefore complements previously reported descriptions of the hydrodynamic load

dx.doi.org/10.1021/ac4014918 | Anal. Chem. 2013, 85, 8676−8683

$$\Gamma = (a + b\cdot\mathcal{R}[\Gamma_{\kappa_n\to\infty}(Re, k_n)]) + i(Re^{-c} + d\cdot\mathcal{I}[\Gamma_{\kappa_n\to\infty}(Re, k_n)]) \text{ for } Re \geq 10^3 \quad (3)$$

$$\Gamma_{\kappa_n\to\infty} = \frac{8}{\pi\kappa_n}\frac{\sqrt{\kappa_n^2 - iRe}}{\sqrt{\kappa_n^2 - iRe} - \kappa_n} \text{ as } \kappa_n \to \infty \quad (4)$$

The approximation is based on the corrected asymptotic solution $\Gamma_{\kappa_n\to\infty}$ from Van Eysden and Sader,[12] valid for higher normalized mode numbers κ_n. The parameters a, b and c, d are correction terms for the real and imaginary components, respectively. The following requirements are fulfilled by the approximation: In the asymptotic limit $Re \to \infty$, the real part of the hydrodynamic function approaches the values of the inviscid theory[32] with good accuracy, whereas the imaginary part reaches zero. Furthermore, the correction terms $a,Re^{-c} \to 0$ and $b,d \to 1$ for $\kappa_n \gg 1$ to recover the asymptotic solution (eq 4). The correction parameters were determined by fitting the real and imaginary part of the approximation to the numerically calculated values in the range $Re = \{10^3, ..., 10^4\}$ and $\kappa_n = \{0.1, ..., 20\}$ and are provided in the Supporting Information. Discrete values of Γ were numerically calculated according to literature[12] for $Re = \{10^0, ..., 10^4\}$ and $\kappa_n = \{0.1, ..., 20\}$. Figure 2

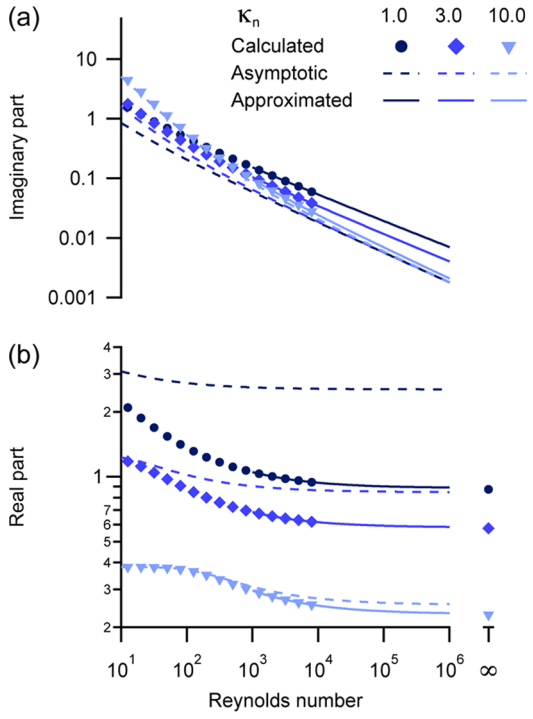

Figure 2. Log–log plot of the imaginary (a) and real (b) part of the hydrodynamic function Γ for various values of the normalized mode number κ_n. Calculated[12] (markers), asymptotic[12] (dashed lines, eq 4) and approximated (solid lines, eq 3) values are shown. For better visibility, every other calculated value has been omitted. The results of the inviscid theory[32] are indicated in the real part (∞).

shows numerically calculated, asymptotic and approximated values of the hydrodynamic function for various κ_n. Because the Reynolds numbers obtained in the experiments are in the order of 10^2 to 10^5, a combination of the numerically calculated and approximated values of the hydrodynamic function was used. The transition region ($Re = \{10^3, ..., 10^4\}$) was described by a linearly weighted average of both functions.

RESULTS AND DISCUSSION

A microcantilever based method for fluid viscosity and mass density measurements with high temporal resolution and microliter sample consumption is presented (Figure 1). The measurements are achieved by monitoring higher flexural mode vibrations of a cantilever immersed in the liquid under test. The measuring principle is depicted in Figure 3. In the following, we present (i) the dynamics of vibrating microcantilevers driven by optical excitation in liquid, (ii) the validation of the instrument performance with liquids of known viscosity and mass density, (iii) an optimized sample delivery procedure involving a two-phase flow, and (iv) the application of the sensor to characterize chemical polymerization reactions.

Photothermal Excitation of Resonating Cantilevers in Liquid. The phase and amplitude response of a resonating cantilever immersed in liquids of different viscosity and mass density, namely, water and glycerol solutions, are shown in Figure 4. The cantilever was embedded in a molded fluid cell with a volume below 2 μL. Vibration was induced photothermally and detected using an optical beam deflection setup (Figure 1). The high spring constants of the cantilevers[35] and the viscous surroundings require efficient excitation to drive higher flexural modes at a detectable amplitude. Photothermal excitation allows cantilever vibration to be induced without mechanical contact.[36,37] Thus, the excitation system is completely separated from the fluid cell. To ensure efficient photothermal excitation of higher flexural modes, the excitation laser was positioned close to the clamped end of the cantilever beam, where the curvature is highest. In contrast, the detection laser was focused at the free end of the cantilever, where maximal angular deflection occurs. Furthermore, the efficiency was improved by matching the excitation and detection laser wavelengths to the absorption properties of the cantilever coating,[38] in this case gold. At the excitation wavelength of 406 nm, the absorption of gold is about 67%,[39] allowing efficient heating that is in turn transduced into a bending moment. In contrast, the absorption of gold is <3% (reflectivity >97%)[39] at 780 nm rendering this wavelength suitable for the detection laser. Advantages of photothermal excitation are (i) undisturbed resonance spectra, (ii) suitable integration into microfluidics, (iii) scalability, for example, scanning over arrays of cantilevers, and (iv) separation of the excitation and detection system from microfluidics, allowing flexible fluid cell designs. Potential drawbacks of photothermal excitation and optical detection include the following: (i) Only applicable to optically transparent sample fluids, (ii) requires a two-step alignment, and (iii) local fluid heating (see Supporting Information).

The resonance spectra shown in Figure 4 are free of any spurious resonances. The phase and amplitude response of a cantilever is an entanglement of various effects depending on (i) the properties of the fluid, that is, increasing viscosity and mass density decrease the quality factor, shift the eigenfrequencies toward lower values and reduce the amplitude of vibration; the shifts are more pronounced for higher modes, (ii) the mechanical properties and dimensions of the cantilever, (iii) the position, thermal lag and the spot size of the photothermal excitation, (iv) the phase-lag and bandwidth (850 kHz) of the electronics, and (v) the degree of angular bending, that is, the stronger angular bending of higher flexural modes increases the response detected in the optical beam deflection system.

dx.doi.org/10.1021/ac4014918 | Anal. Chem. 2013, 85, 8676–8683

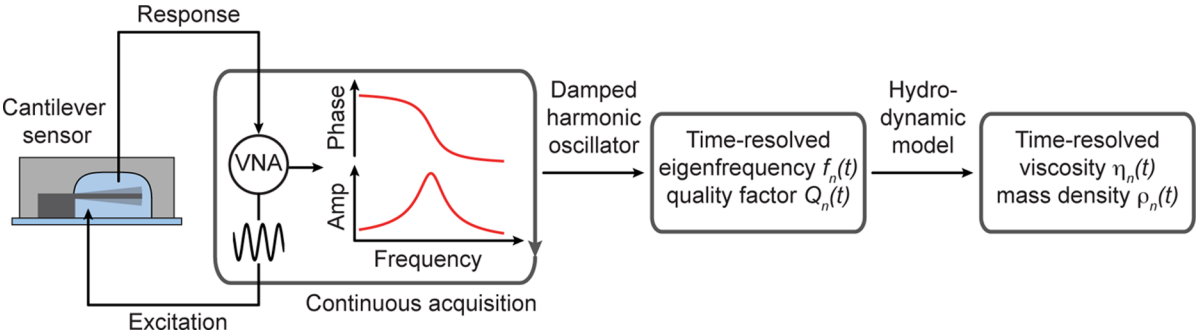

Figure 3. Measuring principle: A vector network analyzer (VNA) applies a frequency swept excitation signal to the immersed cantilever sensor and detects its response. Resulting phase and amplitude spectra are acquired continuously. Time-resolved values of the eigenfrequency f_n and quality factor Q_n are determined by fitting a damped harmonic oscillator model to the spectra. The values are converted into viscosity and mass density data by using a hydrodynamic model, which quantifies the cantilever–fluid interactions (see Materials and Methods).

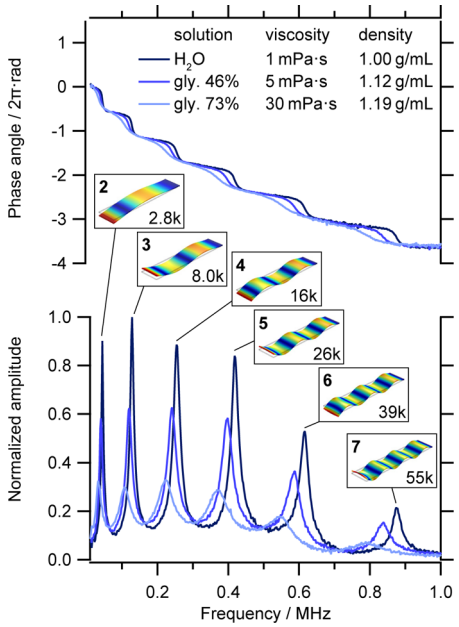

Figure 4. Phase and amplitude response of a photothermally driven cantilever (500 × 100 × 4 μm^3) immersed in liquids of different viscosity and mass density, namely water (H_2O) and glycerol solutions (gly. wt %). The flexural mode number (bold), the corresponding Reynolds number in water and the mode shape are indicated above the resonance peaks. Note the absence of spurious resonances. The first flexural mode is not visible due to high-pass filtering. The angular deflection amplitude is normalized to the highest peak.

Viscosity and Mass Density Measurements of Reference Fluids. After calibration in water (1.01 mPa·s, 998 kg/m^3; average of 10 spectra) at the start of a flow-through measurement, viscosities and mass densities of the sample fluids were calculated from the measured eigenfrequencies and quality factors. Mass density mainly affects the comoving mass and thus the eigenfrequency of the resonator. In contrast, viscous forces alter the dissipation and thus govern the quality factor. The influence of the viscosity on the eigenfrequency is due to the boundary-layer thickness[40] which extends further for lower modes, and thus increases the comoving mass.

A calibration step is essential to avoid systematic errors. Deviations of the vacuum frequency from the calculated values are mainly caused by the uncertainty in the average thickness of the cantilevers, and become more pronounced at higher modes.[41] The quality factor is affected by various dissipative mechanisms. For the cantilevers employed, viscous dissipation dominates by orders of magnitude.[42] Because only fluid in closest vicinity to the cantilever is probed, that is, within the viscous boundary layer,[40] local heating effects originating from the incident lasers must be considered. Finite element analysis suggests that the average heating inside the probed fluid volume (<1 nL) is below 2.3 K (see Supporting Information). Because the viscosity has a stronger temperature dependence than the mass density,[43] an increase in temperature mainly alters the quality factor. To account for these interfering effects, the vacuum frequency and a quality factor calibration constant were determined using water as a calibration fluid.

Figure 5 shows measured viscosity and mass density values of reference fluids (glycerol solutions) derived from the different

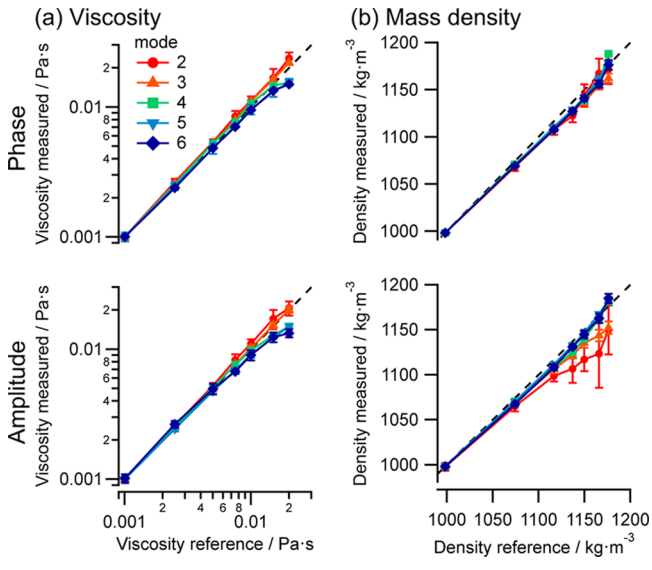

Figure 5. (a) Viscosity and (b) mass density values of glycerol solutions, derived from the amplitude (bottom) and phase (top) response of flexural modes 2–6, after calibration in water. Reference values are indicated by the dashed lines.[26,27] The data points show the mean and standard deviation derived from 10 spectra.

flexural modes. The analysis was performed for the phase, as well as for the amplitude spectra. The accuracy is mainly governed by the peak amplitude, which defines the signal-to-noise ratio. In general, higher modes show less variance because of the larger absolute shifts in eigenfrequency and quality factor. At high viscosities, values derived from higher modes deviate

dx.doi.org/10.1021/ac4014918 | Anal. Chem. 2013, 85, 8676–8683

from the reference values. Because of the larger absolute shifts observed at higher modes, the response saturates more rapidly impairing accurate determination of the viscosity values. The deviations in mass density derived from amplitude spectra of lower modes are due to the decreasing peak amplitudes, which hinders the precise determination of the eigenfrequency. After a single reference calibration in water, quantitative viscosity measurements performed on the reference fluids were accurate to within 25% (phase) and 34% (amplitude) in a range from 1 to 20 mPa·s (12% (phase) and 10% (amplitude) for 1−10 mPa·s). Mass density values were determined within 1% (phase) and 4% (amplitude) from 998 to 1176 kg/m^3. These values are comparable[18] or better[44] than the ones reported for similar viscosity ranges using cantilevers. The more the sample characteristics deviated from those of the calibration fluid and the higher the viscosity, the more the measured values differed from literature values and the larger the standard deviations. Better accuracy can be obtained using a multireference calibration[17] or cantilevers with a higher aspect ratio.[20] Furthermore, the precision can be adjusted by adapting the cantilever dimensions to a certain measurement range.

Segmented Two-Phase Flow to Avoid Sample Dispersion. Dilution of the sample by dispersion into an aqueous carrier fluid leads to deviations in viscosity and mass density. Such Taylor dispersion[45] increases with the initial solute concentration and the flow rate. Therefore, efficient delivery of the sample liquid to the sensor is crucial for accurate measurements in flow-through instruments. The use of an oil phase as carrier fluid,[46] which effectively prevents sample dilution, allows smaller sample volumes to be measured. As illustrated in Figure 6, the use of a hydrocarbon oil resulted in a segmented two-phase flow, allowing fast and reliable screening of samples as small as 5 μL. Measured viscosity and mass density values are in good agreement with literature values (dashed lines[26,27]) for both the carrier and the samples.[45] Furthermore, the measured values returned to the baseline immediately after each sample plug, clearly indicating that there was no unspecific adsorption to the cantilever. During sample injection and purging the laser beams are scattered because of (i) the different refractive indices of the fluids and (ii) interfacial forces deflecting the cantilever, leading to a temporary decrease in laser intensity. To account for this, data points recorded below a certain laser intensity threshold were excluded from the analysis (see Supporting Information). In summary, miniaturization and optimized liquid handling significantly improved the sensor characteristics. These findings might also be applicable to other transducer technologies.

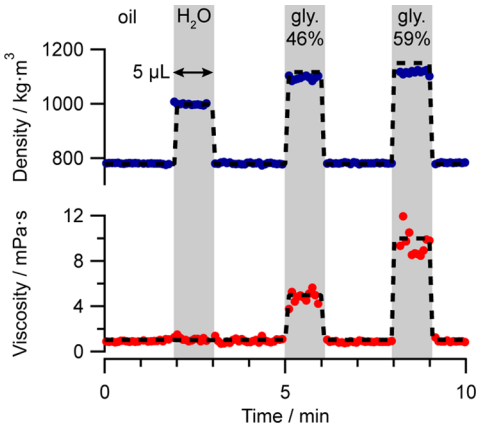

Figure 6. Viscosity and mass density values derived from the 4th flexural mode upon sequential injection of 5 μL samples using a hydrocarbon oil as carrier fluid. The use of a hydrophobic carrier phase prevents dispersion and thus delivers the sample to the cantilever transducer at its initial concentration. After calibration in the carrier fluid (oil), water (H_2O) and different glycerol solutions (gly. wt %) were injected. Reference values are indicated by the dashed lines.[26,27]

Real-Time Monitoring of Free Radical Polymerization Reactions. The polymerization of acrylamide was selected as a model system to demonstrate the study of dynamic processes and to validate the results delivered by the sensor by comparing them to published rheokinetic data.[47] The specific viscosity of a polyacrylamide (PAa) solution η_{sp} is proportional to the polymer concentration c and the viscosity average molar mass $\bar{M}_v$ according to $\eta_{sp} \propto c^6\bar{M}_v^{3.4}$.[47] This equation can be expanded into a rheokinetic model that links the measured viscosity at any given reaction time to the monomer-to-polymer conversion of the reaction (see Supporting Information and ref 47).

Figure 7a shows time-resolved viscosity and mass density data derived from flexural modes 2−6. After recording a stable baseline in acrylamide monomer solution, the reaction was initiated by adding ammonium persulfate (+APS). As atmospheric oxygen was present, the reaction started after a lag-phase (t_0). Viscosity hardly increased in the initial polymerization phase because of the weak viscosity-concentration dependence at low polymer concentrations. A strong increase in viscosity was observed in the next stage, that is, at higher polymer concentrations, until saturation, which was reached when most monomer had been converted into polyacrylamide. The difference in the absolute cantilever response in the polyacrylamide solution (PAa, Figure 7a) is explained by the occurrence of shear-thinning at higher frequencies. The measured mass density deviated toward lower values, even though an increase was expected (see Supporting Information). The employed hydrodynamic model does not account for the non-Newtonian behavior of the solution,[12] therefore misinterpreting shear-thinning as a decrease in mass density. The deviation becomes more pronounced at lower modes, where the eigenfrequency strongly depends on an entanglement of viscosity and mass density. In contrast, the eigenfrequencies of higher modes are almost independent of the viscosity and, thus, reproduce the mass density with higher accuracy.

To validate the use of the sensor for kinetic measurements, a rheokinetic model[47] was fitted to the viscosity data (Figure 7a, solid black lines; see Supporting Information for details). The rheokinetic model describes the measured data well and was used to calculate the degree of conversion β of the reaction over time as shown in Figure 7b. In the initial stage (β < 25%) of the polymerization, it cannot be accurately determined due to the weak viscosity-concentration dependence. Even though shear-thinning occurred, the determined degrees of conversion are consistent along all modes. As expected for a free radical polymerization,[47] the degree of conversion is well described by a first order kinetic with a second order initiation reaction (solid black lines in Figure 7b). The degree of conversion at the end of the reaction additionally determined by ^{1}H NMR was (96 ± 2)%. In good agreement, the rheokinetic model extrapolated to 95% (Figure 7b). These results approve the use of nanomechanical cantilevers to monitor the kinetics of polymerization reactions solely by measuring changes in viscosity.

dx.doi.org/10.1021/ac4014918 | Anal. Chem. 2013, 85, 8676−8683

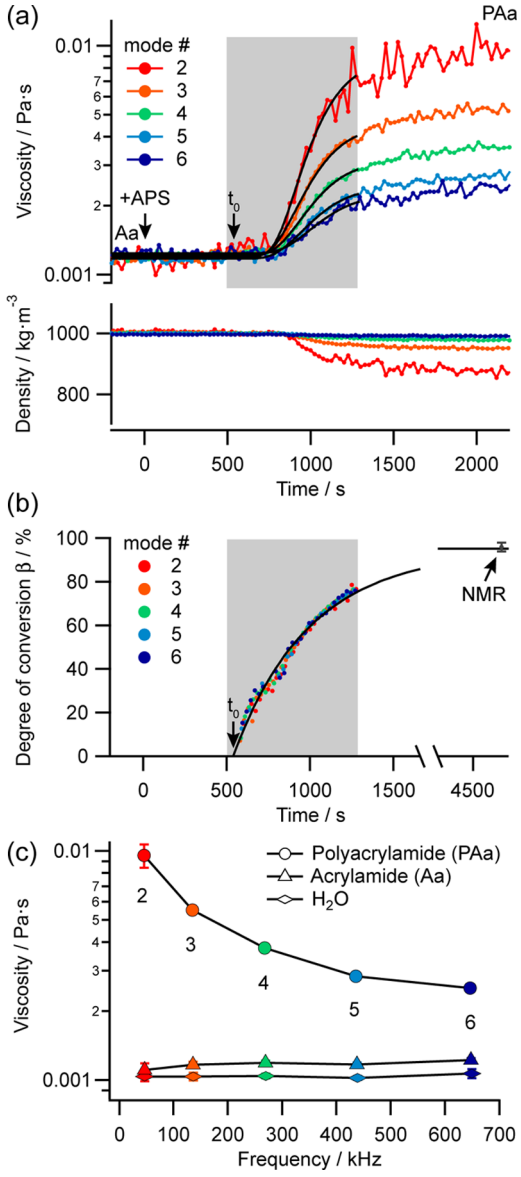

Figure 7. Free radical polymerization of acrylamide. (a) Viscosity and mass density data derived from phase spectra. The acrylamide solution (Aa) was initiated with ammonium persulfate (+ APS). After a lag-phase (t_0) due to the presence of oxygen, the reaction started and the viscosity increased until the monomer became depleted (PAa). (b) The degree of conversion during the reaction (gray area) was determined by fitting rheokinetic models[47] to the viscosity data (solid black lines in a). It is well described by a first order kinetics with a second order initiation reaction (solid black line in b). The degree of conversion at the end of the reaction was furthermore determined by ^{1}H NMR. (c) Frequency dependent viscosity of the polymer solution (polyacrylamide), the monomer solution (acrylamide), and water (H_2O; mode numbers are indicated).

Figure 7c shows the shear-thinning behavior of the polymer solution (PAa)[48] determined at the end of the reaction. In contrast, the monomer solution (Aa) and the solvent (H_2O) displayed Newtonian (frequency independent) behavior. Recently introduced theoretical models for the characterization of viscoelastic fluids using microcantilevers account for such non-Newtonian behavior. However, they only consider the fundamental flexural mode and require prior knowledge of the mass density.[49] Extending such models to higher modes would enable viscoelastic behavior to be characterized over a wide range of frequencies.

CONCLUSIONS

The method presented uses nanomechanically resonating cantilevers to achieve quantitative, time-resolved fluid viscosity and mass density measurements. The implemented photothermal excitation method avoided spurious resonances and allowed integration of the sensor into PDMS microfluidics, where piezoelectric excitation is unsuitable.[50] Embedding the cantilever transducer in a microfluidic PDMS cell and implementing a two-phase fluidic system avoided sample dispersion, allowing measurements to be reproducibly made with 5 μL sample volumes. The hydrodynamic model of Van Eysden and Sader[12] was adapted to allow higher flexural modes, that is, vibration at high Reynolds numbers, to be considered. The extended model was validated using Newtonian reference solutions prepared from glycerol.

Using the microcantilever based instrument it was possible to follow the free radical polymerization of acrylamide in a time-resolved manner with a total sample consumption of just 75 μL during 65 min. Non-Newtonian shear-thinning behavior observed in the viscosity data revealed limitations of the theoretical framework employed, impairing accurate determination of the mass density, especially at lower modes of vibration. Despite the observed shear-thinning, the degree of monomer-to-polymer conversion was determined using rheokinetic models,[47] and was consistent for all modes of vibration. In future, the instrument could be used to determine the kinetic constants of unknown reactions. Further, the very small sample volumes required make it ideally suited to monitor polymerization kinetics in microreactors[51] or in reactions that have to be conducted on a very small scale, for example, to explore the parameters for expensive (bio)-catalysts.[52] In addition to its use to characterize chemical polymerization reactions, the presented sensor should allow biological aggregation processes to be investigated.

ASSOCIATED CONTENT

Supporting Information

Eigenfrequencies, quality factors, and calibration parameters; tabulated correction parameters for the approximation of the hydrodynamic function; finite element analysis of the laser induced increase in temperature; data analysis of two-phase flow experiments; analysis of the acrylamide polymerization by rheokinetic models. This material is available free of charge via the Internet at http://pubs.acs.org/.

AUTHOR INFORMATION

Corresponding Author

*E-mail: thomas.braun@unibas.ch. Phone: +41 (0)61 387 32 28. Fax: +41 (0)61 387 39 86.

Notes

The authors declare no competing financial interest.

ACKNOWLEDGMENTS

The authors gratefully acknowledge Henning Stahlberg (C−CINA, University of Basel) for providing infrastructure and facilities; Shirley A. Müller (C−CINA, Univ. Basel) for critically reading the manuscript; Bernd Rinn (CISD, D-BSSE, ETHZ) and Patrick Vogt (URZ, Univ. Basel) for support with numerical calculations; François Huber and Natalija Backmann

(SNI, Univ. Basel) for help with the sensor passivation; Andreas Hierlemann and Alexander Stettler (BEL, D-BSSE, ETHZ) for assistance on PDMS fabrication; Andreas Tonin (Electronics Workshop, Dept. Physics, Univ. Basel) and Raymond Strittmatter (Mechanical Workshop, Biozentrum, Univ. Basel) for helping to design the instrument and for its manufacture; Michel Despont and Ute Drechsler (IBM Research GmbH, Rüschlikon, Switzerland) for providing cantilever arrays; Thomas Pfohl (Department of Chemistry, Univ. Basel) and Ernst Meyer (Dept. Physics, Univ. Basel) for fruitful discussions. This work was supported by SNF grant 200021/130594, NCCR Nano, and ARGOVIA project NoViDeMo.

REFERENCES

(1) Lee, J.; Tripathi, A. *Anal. Chem.* **2005**, *77*, 7137−7147.
(2) Pipe, C. J.; McKinley, G. H. *Mech. Res. Commun.* **2009**, *36*, 110−120.
(3) Sparks, D.; Smith, R.; Straayer, M.; Cripe, J.; Schneider, R.; Chimbayo, A.; Anasari, S.; Najafi, N. *Lab Chip* **2003**, *3*, 19−21.
(4) Zhang, J.; Dai, C.; Su, X.; O'Shea, S. J. *Sens. Actuators, B* **2002**, *84*, 123−128.
(5) Sparks, D.; Smith, R.; Cruz, V.; Tran, N.; Chimbayo, A.; Riley, D.; Najafi, N. *Sens. Actuators, A* **2009**, *149*, 38−41.
(6) Riesch, C.; Reichel, E. K.; Jachimowicz, A.; Schalko, J.; Hudek, P.; Jakoby, B.; Keplinger, F. *J. Micromech. Microeng.* **2009**, *19*, 075010.
(7) Ricco, A. J.; Martin, S. J. *Appl. Phys. Lett.* **1987**, *50*, 1474−1476.
(8) Liu, Y.; DiFoggio, R.; Sanderlin, K.; Perez, L.; Zhao, J. *Sens. Actuators, A* **2011**, *167*, 347−353.
(9) Doy, N.; McHale, G.; Newton, M. I.; Hardacre, C.; Ge, R.; MacInnes, J. M.; Kuvshinov, D.; Allen, R. W. *Biomicrofluidics* **2010**, *4*, 014107.
(10) Boskovic, S.; Chon, J. W. M.; Mulvaney, P.; Sader, J. E. *J. Rheol.* **2002**, *46*, 891−899.
(11) Sader, J. E. *J. Appl. Phys.* **1998**, *84*, 64−76.
(12) Van Eysden, C. A.; Sader, J. E. *J. Appl. Phys.* **2007**, *101*, No. 044908.
(13) Chon, J. W. M.; Mulvaney, P.; Sader, J. E. *J. Appl. Phys.* **2000**, *87*, 3978−3988.
(14) Bergaud, C.; Nicu, L. *Rev. Sci. Instrum.* **2000**, *71*, 2487−2491.
(15) Ghatkesar, M. K.; Braun, T.; Barwich, V.; Ramseyer, J.-P.; Gerber, C.; Hegner, M.; Lang, H. P. *Appl. Phys. Lett.* **2008**, *92*, No. 043106.
(16) McLoughlin, N.; Lee, S. L.; Hähner, G. *Lab Chip* **2007**, *7*, 1057−1061.
(17) Hennemeyer, M.; Burghardt, S.; Stark, R. W. *Sensors* **2008**, *8*, 10−22.
(18) Youssry, M.; Belmiloud, N.; Caillard, B.; Ayela, C.; Pellet, C.; Dufour, I. *Sens. Actuators, A* **2011**, *172*, 40−46.
(19) McLoughlin, N.; Lee, S. L.; Hähner, G. *Appl. Phys. Lett.* **2006**, *89*, 184106.
(20) Paxman, R.; Stinson, J.; Dejardin, A.; McKendry, R. A.; Hoogenboom, B. W. *Sensors* **2012**, *12*, 6497−6507.
(21) Kim, S.; Kihm, K. D.; Thundat, T. *Exp. Fluids* **2010**, *48*, 721−736.
(22) Ahmed, N.; Nino, D. F.; Moy, V. T. *Rev. Sci. Instrum.* **2001**, *72*, 2731−2734.
(23) Ghatkesar, M. K.; Rakhmatullina, E.; Lang, H. P.; Gerber, C.; Hegner, M.; Braun, T. *Sens. Actuators, B* **2008**, *135*, 133−138.
(24) Duffy, D. C.; McDonald, J. C.; Schueller, O. J. A.; Whitesides, G. M. *Anal. Chem.* **1998**, *70*, 4974−4984.
(25) Green, C. P.; Sader, J. E. *J. Appl. Phys.* **2005**, *98*, No. 114913.
(26) Cheng, N.-S. *Ind. Eng. Chem. Res.* **2008**, *47*, 3285−3288.
(27) Bosart, L. W.; Snoddy, A. O. *Ind. Eng. Chem.* **1928**, *20*, 1377−1379.
(28) Braun, T.; Barwich, V.; Ghatkesar, M. K.; Bredekamp, A. H.; Gerber, C.; Hegner, M.; Lang, H. P. *Phys. Rev. E* **2005**, *72*, No. 031907.
(29) Van Eysden, C. A.; Sader, J. E. *J. Appl. Phys.* **2009**, *106*, No. 094904.
(30) Van Eysden, C. A.; Sader, J. E. *Phys. Fluids* **2006**, *18*, No. 123102.
(31) Vančura, C.; Dufour, I.; Heinrich, S. M.; Josse, F.; Hierlemann, A. *Sens. Actuators, A* **2008**, *141*, 43−51.
(32) Van Eysden, C. A.; Sader, J. E. *J. Appl. Phys.* **2006**, *100*, No. 114916.
(33) Maali, A.; Hurth, C.; Boisgard, R.; Jai, C.; Cohen-Bouhacina, T.; Aimé, J.-P. *J. Appl. Phys.* **2005**, *97*, No. 074907.
(34) Aureli, M.; Basaran, M. E.; Porfiri, M. *J. Sound. Vib.* **2012**, *331*, 1624−1654.
(35) Kokavecz, J.; Mechler, A. *Phys. Rev. B* **2008**, *78*, No. 172101.
(36) Ramos, D.; Tamayo, J.; Mertens, J.; Calleja, M. *J. Appl. Phys.* **2006**, *99*, No. 124904.
(37) Fukuma, T. *Rev. Sci. Instrum.* **2009**, *80*, No. 023707.
(38) Nishida, S.; Kobayashi, D.; Kawakatsu, H.; Nishimori, Y. *J. Vac. Sci. Technol. B* **2009**, *27*, 964−968.
(39) Johnson, P. B.; Christy, R. W. *Phys. Rev. B* **1972**, *6*, 4370−4379.
(40) Batchelor, G. K. *An Introduction to Fluid Dynamics*; Cambridge University Press: Cambridge, U.K., 1967.
(41) Ghatkesar, M. K.; Barwich, V.; Braun, T.; Ramseyer, J.-P.; Gerber, C.; Hegner, M.; Lang, H. P.; Drechsler, U.; Despont, M. *Nanotechnology* **2007**, *18*, No. 445502.
(42) Lochon, F.; Dufour, I.; Rebiere, D. *Sens. Actuators, B* **2006**, *118*, 292−296.
(43) Kim, S.; Kihm, K. D. *Appl. Phys. Lett.* **2006**, *89*, No. 061918.
(44) Wilson, T. L.; Campbell, G. A.; Mutharasan, R. *Sens. Actuators, A* **2007**, *138*, 44−51.
(45) Squires, T.; Quake, S. R. *Rev. Mod. Phys.* **2005**, *77*, 977−1026.
(46) Seemann, R.; Brinkmann, M.; Pfohl, T. *Rep. Prog. Phys.* **2012**, *75*, No. 016601.
(47) Kulichikhin, S. G.; Malkin, A. Y.; Polushkina, O. M.; Kulichikhin, V. G. *Polym. Eng. Sci.* **1997**, *37*, 1331−1338.
(48) Kulicke, W. M.; Kniewske, R.; Klein, J. *Prog. Polym. Sci.* **1982**, *8*, 373−468.
(49) Youssry, M.; Lemaire, E.; Caillard, B.; Colin, A.; Dufour, I. *Meas. Sci. Technol.* **2012**, *23*, No. 125306.
(50) Ricciardi, C.; Canavese, G.; Castagna, R.; Ferrante, I.; Ricci, A.; Marasso, S. L.; Napione, L.; Bussolino, F. *Biosens. Bioelectron.* **2010**, *26*, 1565−1570.
(51) Bhangale, A. S.; Beers, K. L.; Gross, R. A. *Macromolecules* **2012**, *45*, 7000−7008.
(52) Sigg, S. J.; Seidi, F.; Renggli, K.; Silva, T. B.; Kali, G.; Bruns, N. *Macromol. Rapid Commun.* **2011**, *32*, 1710−1715.